



HAL
open science

Modeling hydro-mechanical couplings between interstitial fluids and human skin soft tissues in vivo

Marie-Angèle Abellan, Jean-Michel Bergheau, Hassan Zahouani

► **To cite this version:**

Marie-Angèle Abellan, Jean-Michel Bergheau, Hassan Zahouani. Modeling hydro-mechanical couplings between interstitial fluids and human skin soft tissues in vivo. CFM 2015 - 22ème Congrès Français de Mécanique, Aug 2015, Lyon, France. hal-03445003

HAL Id: hal-03445003

<https://hal.science/hal-03445003>

Submitted on 23 Nov 2021

HAL is a multi-disciplinary open access archive for the deposit and dissemination of scientific research documents, whether they are published or not. The documents may come from teaching and research institutions in France or abroad, or from public or private research centers.

L'archive ouverte pluridisciplinaire **HAL**, est destinée au dépôt et à la diffusion de documents scientifiques de niveau recherche, publiés ou non, émanant des établissements d'enseignement et de recherche français ou étrangers, des laboratoires publics ou privés.

Modeling hydro-mechanical couplings between interstitial fluids and human skin soft tissues in vivo

M-A. ABELLAN^a, J-M. BERGHEAU^a, H. ZAHOUANI^a

a. Université de Lyon, ENISE LTDS UMR 5513 CNRS, 58 rue Jean Parot,
F42023 Saint-Etienne, France. marie-angele.abellan@enise.fr

Résumé :

La peau humaine est formée de cellules, de tissus et de systèmes circulatoires baignés par des fluides physiologiques interstitiels qui leur apportent les nutriments et qui emportent les déchets. L'homéostasie est maintenue par les échanges continuels entre ces différentes entités. Ces échanges sont influencés par la réponse globale de la peau aux chargements extérieurs. La compréhension des mécanismes mis en œuvre lors de ces échanges au niveau interstitiel est importante pour l'étude de l'évolution de la peau humaine in vivo. Ce papier propose l'extension d'un travail précédent en vue de la modélisation mathématique des flux de fluides interstitiels couplés à la réponse mécanique des tissus souples de la peau. Basé sur une approche phénoménologique thermo-hydro-mécanique et physico-chimique de milieu hétérogène (THMPC), maintenant le modèle tri-phasique de peau humaine in vivo considère la peau comme un milieu stratifié déformable comportant 4 couches, 4 solides dans la phase solide, 4 fluides interstitiels dans la phase fluide et un composé ionique. Dans chaque couche, le solide est décrit comme un solide linéaire élastique isotrope et le fluide interstitiel est supposé être un fluide visqueux newtonien. De plus pour ce modèle, une relation est élaborée pour estimer la pression du fluide interstitiel de chaque couche couplée au comportement mécanique dans la couche et entre les couches. Des simulations numériques d'essais d'indentation sur peau humaine in vivo sont présentées et comparées aux observations disponibles dans la littérature. L'étude conduit à l'estimation des paramètres mécaniques de chacune des couches de peau prenant en compte l'influence des flux des fluides interstitiels et du transport d'ions à travers ces couches.

Abstract:

It is now well established that human skin consists of cells, tissues, circulatory systems all bathed in interstitial fluids providing them with nutrients and removing their waste products. Homeostasis is maintained by continuous exchanges between these different entities influenced by the overall answer of human skin to external loads. The understanding of interstitial transports is important when studying the evolutions of human skin in vivo. This paper proposes to extend a previous work to derive a mathematical modelling for describing interstitial fluid flow propagation coupled with the mechanical answers of skin soft tissues based on the evaluation of the interstitial fluid pressures within a tri-phasic model of skin in vivo. This model is based on a general phenomenological thermo-hydro-mechanical and physico-chemical (THMPC) approach of heterogeneous media. The skin is seen here as a deforming stratified medium composed of four layers, four solids in the solid phase,

four interstitial fluids in the fluid phase and an ionic component. In each layer, the solid is described by its own linear, elastic isotropic law while the interstitial fluid is treated as a Newtonian viscous fluid. Moreover for this model, a relation is derived for estimating the interstitial fluid pressure within each layer and its couplings with the mechanical behavior within the layer and between layers. Numerical simulations of in vivo indentation test performed in the laboratory on human skin in vivo are given and compared with typical observations of indented human skin available in the literature. The discussion leads to quantitative estimates of the mechanical parameters of each layer of human skin soft tissues taking into account the influence of interstitial fluid flows and ions transports through these layers.)

Keywords: biomechanics, multi-phase media, fluid flow propagation, human skin, transport of ions, indentation test, numerical simulation, interstitial fluid, mechanical parameters.

1 Introduction

The human skin is the largest organ of the human body. It has a major role in providing a barrier against the external environment. The skin prevents excessive water loss from the aqueous interior when exposed to sun or in case of injury, the ingress of undesirable chemical substances and micro-organisms in case of pollution. It provides strength and stiffness to resist mechanical loadings. Human skin interfaces with cosmetic products like creams or personal care devices such as shavers. The skin can be threatened and need to resist to diseases, trauma, medical problems, clinical or aesthetic treatments. It plays an important role in the regulation of the internal temperature of the human body. Human skin is composed of several layers, each with a unique structure and function. These layers are from the skin outer surface inward: the stratum corneum, the viable epidermis, the dermis and the hypodermis [1, 2]. The evolutions and the answers of this barrier vary considerably among the layers and depend on the person, the site on the body, the age, the health, the nutritional status and its state (intact or damaged) [3]. For these reasons, the behavior of the human skin is complex to understand and to model.

The stratum corneum is a dense coating of dead cells while the viable epidermis is an epithelial of soft living cells. The dermis is made up of a network of strong collagen fibres and elastin fibres embedded in a matrix of ground substances. Usually the stratum corneum is quite dry compared with the subsurface hydrated by the interstitial tissue fluid of the underlying dermis. This tissue fluid is a solution that bathes and surrounds the cells of skin soft tissues.

Since the pioneering work of [4] on fluid filtration, developing researches show that the directions of movement of water and solutes through skin layers, by and across blood micro-vessels and lymphatic micro-vessels and their contribution to tissue homeostasis are influenced both by hydrostatic and oncotic (hence protein concentration) pressure differences across the microvasculature walls and by the actively regulated permeability and contractile properties of these vessel walls [5, 6, 7, 8, 9, 10].

These changes can only be evaluated in an in vivo situation. Various techniques have been developed for fluid isolation, as reviewed by [11] and more recently by [12], in search to quantify interstitial Starling forces, as well as the tissue fluid concentration of signalling substances. To a large extent based on Darcy's law, data on the physiological properties of the extracellular matrix and the interstitial transport properties can be found in reference [13]. With respects to mathematical

modelling for understanding interstitial transport, several detailed models of transport properties have been developed [14, 15, 16].

Moreover studies of the mechanical behavior of the skin have shown that the human skin is a stratified non-homogeneous, anisotropic, non-linear viscoelastic material which is subjected to a pre-stress in vivo [17, 18, 19]. This leads to difficulties in obtaining quantitative descriptions of mechanical properties of the skin. Different non-invasive techniques have been developed in the past to evaluate the mechanical properties of skin [20, 21, 22, 23, 24]. Indentation tests are considered here as support for characterizing in vivo equivalent parameters of human skin. They are conducted on the LTDS indentation device which is able to apply a normal load onto the outer surface of the human skin without pre-stressing the skin before the test i.e. without changing its natural stress state [25, 26].

For the simulation of these indentation tests, this paper proposes to extend the theoretical-experimental-numerical set-up proposed in reference [27]. Now in the mathematical model, the interstitial fluid pressures are considered to be the driving forces coupling the interstitial fluid flows and the mechanical behavior of the different layers of skin tissues when subjected to a mechanical external load in presence of a NaCl solution. A relation is derived to follow the evolutions of these interstitial fluid pressures.

We will first present the context of this paper linked to the histology of human skin in vivo. Then the governing equations for a deforming tri-phasic medium are given and the relation describing the interstitial fluid pressure of the interstitial fluid is derived. The non-invasive experimental device is briefly presented. A finite difference analysis is carried out for a specimen of skin and the obtained numerical results are discussed. Some concluding remarks end the paper.

2 Histology of skin

Typically, an organ like skin consists of parenchymal cells, the circulatory system (including the blood and lymphatic systems), the loose connective tissues (also called the extracellular matrix that constitutes the framework in which the circulatory system is embedded) and the interstitial fluid (that fills the interstitium i.e. the space located between the capillary walls and the cells and/or between the cells). The amount of interstitium is about 50% of wet weight in skin [10, 28]. The parenchymal cells of skin are classified into four main different types giving skin its stratified structure consisting of four main layers, which are from the skin outer surface inward: stratum corneum, viable epidermis, dermis and hypodermis (Fig. 1). In this complex structure, the following points are retained for the purpose of this paper [1, 29, 30].

2.1 Stratum corneum

The stratum corneum is the most superficial skin layer. This layer is a 10-25 μm thick layer composed of corneocytes held together by lipid bridges and corneosomes in what is commonly referred to as a brick-and-mortar structure. The corneocytes are hexagonal flat non-viable cells rich in hard insoluble keratin proteins. They migrate from the underlying viable epidermis. The intercellular spaces are about 0.1-0.3 μm and only 10% bounded water is found in the lipid mortar. Because of its structure and composition, the stratum corneum acts as a protective barrier.

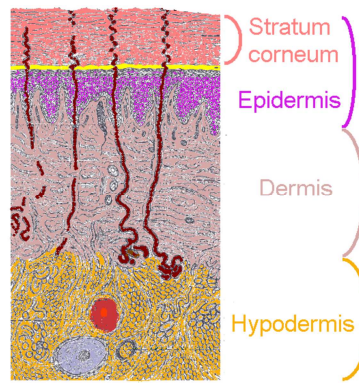


FIGURE 1: Schematic view of the cross-section of human skin showing the distinct layers.

2.2 Viable epidermis

The viable epidermis is a stratified squamous epithelial (10-100 μm). The bulk of epidermal cells are the viable keratinocytes, which migrate upwards to the skin surface and become dead corneocytes. The viable epidermis is a non-vascular structure which also contains melanocytes, Langerhans cells and Merkel cells. Cells are surrounded, nourished and bathed by the interstitial fluid originating in the underlying dermis and transported across the epidermal-dermal junction. The cells are communicating by very strong desmosomes in this very compact tissue; the intercellular spaces occupy less than 2% of the volume. Therefore, the mechanical integrity of the viable epidermis is considered to be stronger than other soft tissues.

2.3 Dermis

The dermis is a 1 to 4 mm thick layer which contains microstructures like blood vessels, lymph vessels, nerve endings, sweat glands, sebaceous glands and hair follicles. It is largely composed of a very dense fibre network of collagen, elastin and minute quantities of reticulin within a significant amount of amorphous ground substance, all bathed in interstitial fluid. The amorphous ground substance combined with the water of the interstitial fluid acts as a viscous gel-like material, which does not leak out of the dermis, even under high pressure [30]. This viscous gel combined with the fibrous network contributes to the protection of vessels and cells against mechanical insults [29].

2.4 Hypodermis

The hypodermis is the adipose tissue layer found between the dermis and the muscles. This adipose tissue is a loose association of lipid-filled cells, the white adipocytes, which are held in a framework of collagen fibres. Stored fat is the predominant component of the adipocytes, where the lipid droplet can exceed 50 μm . Adipose tissue has little extracellular matrix compared to other connective tissues and acts as an insulating layer and a protective cushion which can be some millimetres thick.

2.5 Interstitial fluid

The interstitial fluid is the main component of the extracellular fluid which also includes plasma and trans-cellular fluid. It consists of a water solvent containing sugars, salts, fatty acids, amino acids, coenzymes, hormones, oxygen, neurotransmitters as well as waste products from the cells. The particles dissolved in water are referred to as solute in the remaining of this paper. The interstitial fluid provides a means of delivering materials to the cells, as well as removal of metabolic waste and transport of immune cells. The solute concentrations of interstitial fluid are very variable between tissues and within the same tissue, depending upon its functional state. This means that interstitial fluid has a different composition in the different layers of skin soft tissues.

2.6 Sub-cutaneous layers

The underlying sub-cutaneous layers and entities (such as muscles, bones and tendons) are more resistant than the cutaneous layers. The order of magnitude of their mechanical parameters are found in the literature to be above 10^9 Pa in average. These values are bigger than the ones expected for the mechanical parameters of the cutaneous layers. Therefore the choice is done here to consider them as undeformable materials. This means that they are supposed to be non-affected by the outside mechanical load applied onto the outer surface of the skin during the indentation test presented in section 4.

2.7 Consequences on the skin model

As shown in Sub-section 2.1 to 2.5, skin soft tissues are heterogeneous materials consisting of several components. Moreover, [17] speaks of non-linear anisotropic hyper-elastic and viscoelastic materials. The choice is made here to model skin as a stratified material with four layers. Each skin layer is a different solid material. Based on the observation that each layer has a different composition for its interstitial fluid, it is proposed to consider four different interstitial fluids, one for each layer. Moreover, each solid material is supposed to be saturated by its interstitial fluid i.e. in the solid the interstitial fluid is at its normal content in normal life conditions (edematous cases are not taken into account here) and dissolved gases are considered as part of the interstitial fluid.

The specimen of skin studied in the following paragraphs and given in Fig. 2 considers that:

- the skin specimen is a stratified tri-phasic material with four layers, four solids in the solid phase, four fluids in the fluid phase and an ionic component.
- The four layers are: layer 1 accounts for the stratum corneum, layer 2 for the viable epidermis, layer 3 for the dermis and layer 4 for the hypodermis. They are respectively denoted L_1 , L_2 , L_3 and L_4 in the following.
- The four solids for the solid phase are: solid 1 simulates the corneocytes and the lipid mortar present in the stratum corneum, solid 2 simulates the evolving cells of the viable epidermis, solid 3 simulates the different cells of the dermis including the fiber networks, the lymph and blood vessels as well as the others skin microstructures and solid 4 simulates the fatty connective tissue of the hypodermis. They are respectively denoted s_1 , s_2 , s_3 and s_4 in the following.
- The four fluids for the fluid phase are: fluid 1 simulates the 10% bound water in the lipid mortar of the stratum corneum, fluid 2 simulates the interstitial fluid in the viable epidermis, fluid 3 simulates the interstitial fluid in the dermis and fluid 4 simulates the interstitial fluid in the hypodermis. They are respectively denoted f_1 , f_2 , f_3 and f_4 in the following.
- An ionic component (i) deposited at the outer surface of the skin and of which it can be interesting to follow the penetration.

3 Theoretical model

Based on the general phenomenological thermo-hydro-mechanical and physico-chemical approach of heterogeneous media described in reference [31], the skin model detailed here after considers non-ideal constituents i.e. the behavior of each individual component depends on the behavior of all the other components present in the human skin specimen introduced in paragraph 2.6 (Fig. 2). Therefore interactions need to be taken into account and the field equations are derived under the following assumptions:

- the overall material behavior of the studied specimen of skin is a combination of the behavior of each individual component;

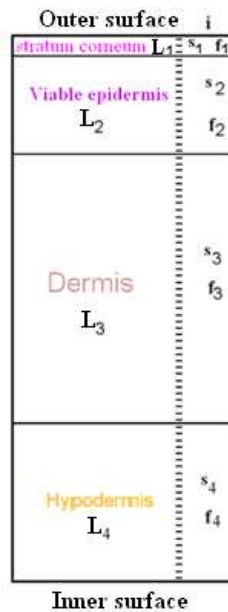


FIGURE 2: Schematic view of the cross-section of the skin specimen showing the four layers: stratum corneum, viable epidermis, dermis, and hypodermis as well as the 9 components: the 4 solids, the 4 fluids and the ions.

- in each infinitesimal volume of heterogeneous medium a finite number of components are present;
- each component contributes to the total material behavior in the same proportion as its volumetric participation given by its volumic ratio;
- all the components are extended to the total studied unit volume of the human skin specimen.
- the reference domain of the human skin specimen coincides with the initial configuration of the skin solids.
- all physical quantities are represented by state variables which are scalars or vectors or tensors function of the Euler variables (\mathbf{x}, t) where t is the time and \mathbf{x} is the spatial vector defining the position of the material particle in the current configuration at time t ;
- the nine constituents, introduced in paragraph 2.6, are referred to with the subscript π and the four layers with the subscript $L\pi$. In the remaining of the paper, $\pi = s_1, s_2, s_3, s_4, f_1, f_2, f_3, f_4, i$ and $L\pi = L_1, L_2, L_3, L_4$ if it is not stated differently.
- all the constituents are inert which means that there is no mass transfer and no chemical reactions between the constituents. Therefore the source of mass of one constituent coming from the other constituents present in the specimen equals zero;
- each solid is treated as isotropic linear solid material described by its own behavior law;
- the four layers are supposed to be made of fluid-saturated materials, i.e. there is only a solid and a fluid phase in each layer, no gas;
- each layer is saturated by its own fluid material seen as a Newtonian viscous fluid with its own behavior law.

- the solute in the interstitial fluids may induce not negligible electrical effects within the skin specimen. In spite of that, we make the choice in this study to focus first on the mechanical ions-fluids-solids couplings and not to take the electrical effects into account;
- the constituents are considered as intrinsically incompressible which means that the absolute mass density $\rho'_\pi(\mathbf{x}, t)$ of constituent π in $\text{kg}\cdot\text{m}^{-3}$ is constant for all constituents;
- the temperature is supposed to be constant all along the study. This assumption is reasonable with respect to the experimentation procedure which imposes a constant ambient temperature in the room all along the tests.

3.1 Balance equations

For inert constituents, as it is the case here, the balance of mass for each constituent π simplifies to:

$$\frac{\partial}{\partial t} \rho_\pi + \text{div} [\rho_\pi v_\pi] = 0 \quad (1)$$

with $v_\pi(\mathbf{x}, t)$ absolute velocity of constituent π in $\text{m}\cdot\text{s}^{-1}$, $\rho_\pi(\mathbf{x}, t)$ relative mass density of constituent π in $\text{kg}\cdot\text{m}^{-3}$ defined by

$$\rho_\pi = n_\pi \rho'_\pi \quad (2)$$

where $n_\pi(\mathbf{x}, t)$ is the volumic ratio of constituent π . Further, the sum of volumic ratios over the constituents present in the medium should equal one

$$n_{s1} + n_{s2} + n_{s3} + n_{s4} + n_{f1} + n_{f2} + n_{f3} + n_{f4} + n_i = 1 \quad (3)$$

Neglecting inertia forces, convective terms and the gravity acceleration, the balance of linear momentum for each constituent π reduces to:

$$\text{div} \sigma_\pi + p'_\pi = 0 \quad (4)$$

with $\sigma_\pi(\mathbf{x}, t)$ the Cauchy stress tensor of constituent π in Pa, $p'_\pi(\mathbf{x}, t)$ the source of momentum for constituent π coming from the other constituents in $\text{kg}\cdot\text{m}^{-2}\cdot\text{s}^{-2}$, which takes into account the possible local drag interactions between the solids, the fluids and the ions and which satisfies the momentum production constraint:

$$p'_{s1} + p'_{s2} + p'_{s3} + p'_{s4} + p'_{f1} + p'_{f2} + p'_{f3} + p'_{f4} + p'_i = 0 \quad (5)$$

3.2 Material relations

Although supposed to be chemically inert in the model, the fluids, ions and solids interact together and there is the need of material relations in addition to the above balance equations. The relations expressing the chemical potentials of the interstitial fluids π (for $\pi=f_1, f_2, f_3, f_4$) encompass these ions-fluids-solids interactions and read

$$\mu_\pi = p_\pi - \Pi_\pi + \psi_\pi \quad (6)$$

where $p_\pi(\mathbf{x}, t)$ is the interstitial fluid pressure of the interstitial fluid π in Pa, $\psi_\pi(\mathbf{x}, t)$ is the matrix potential for the interstitial fluid π accounting for fluids-solids interactions (capillary and adsorptive effects) in Pa, $\Pi_\pi(\mathbf{x}, t)$ is the osmotic pressure for the interstitial fluid π accounting for fluids-ions interactions in Pa. The chemical potentials of the fluids are in $\text{J}\cdot\text{m}^{-3}$. All these quantities (the interstitial fluid pressure $p_\pi(\mathbf{x}, t)$, the matrix potential $\psi_\pi(\mathbf{x}, t)$ and the osmotic pressure $\Pi_\pi(\mathbf{x}, t)$ of fluid π need to be experimentally determined in order to write a close mathematical problem. But it is quite difficult to obtain informations on these physical quantities for the entire specimen of skin when considering it as a homogeneous medium. It is even more difficult to characterize them separately for

each interstitial fluid independently of the other ones. In this paper we propose to deal with by assuming:

- first, a unique form of relation for the matrix potential valid for each interstitial fluid π (for $\pi=f_1, f_2, f_3, f_4$). Following reference [32], the matrix potential depends on the concentration of the ions per unit fluid volume

$$\Pi_\pi = \Pi = 2 R T c_i \quad (7)$$

with R the universal gas constant in $\text{J.K}^{-1}.\text{mol}^{-1}$, T the absolute temperature in $^\circ\text{K}$, $c_i(\mathbf{x}, t)$ the concentration of the ions per unit fluid volume in mol.m^{-3} .

- then the following relation (8) giving the sum $p_\pi + \psi_\pi$ as a function of the volumic ratio n_π of the interstitial fluid π (for $\pi=f_1, f_2, f_3, f_4$). This proposal is based on the observation (see section 2) that the size of the interstitial space is really different from one layer to the other and can be taken as a characteristic of the interstitial fluid of one layer. Following [32], this relation reads

$$p_\pi + \psi_\pi = \left(\exp\left((9.7) \cdot 10^{-5}\right) - \exp\left(\frac{(9.7) \cdot 10^{-5}}{n_f}\right) \right) (9.84) \cdot 10^{10} \quad (8)$$

For the ionic component, the chemical potential $\mu_i(\mathbf{x}, t)$ is defined as

$$\mu_i = \mu_{i0} + RT \ln(c_i) \quad (9)$$

with μ_{i0} chemical potential of the ions in a reference state in J.m^{-3} .

When neglecting couplings between velocity and heat flux, fluid flow through a saturated porous medium with an ionic component is governed by a generalized Darcy's law. It expresses the velocity of the interstitial fluid π (for $\pi=f_1, f_2, f_3, f_4$) in terms of the gradient of the chemical potential $\mu_\pi(\mathbf{x}, t)$ of the interstitial fluid π and the gradient of the chemical potential $\mu_i(\mathbf{x}, t)$ of the ions:

$$n_\pi(v_\pi - v_{s\pi}) = -K_\pi \left[\nabla \mu_\pi + \frac{n_i}{n_\pi} \nabla \mu_i \right] \quad (10)$$

with $v_{s\pi}$ velocity field of the solid present in the layer of the studied interstitial fluid π , $K_\pi(\mathbf{x}, t)$ second-order permeability tensor, it has the unit $\text{m}^4.\text{N}^{-1}.\text{s}^{-1}$. The permeability tensor appearing in equation (10) depends on the interstitial fluid π (for $\pi=f_1, f_2, f_3, f_4$), the permeability of the solid of the layer and the permeability of the capillary and lymphatic walls within the tissue. It has been observed that fluid migration parameters are of varying magnitude by tissue type and vascularization i.e. they are very low in poorly vascularized adipose tissue and high in well vascularized porous tissue [15].

The diffusion of ions through the fluid phase of a porous medium is taken into account through Fick's law. The velocity of the ions is governed by the velocity of the interstitial fluid filling the interstitial space of the skin layer through which the ions are transported and depends on the chemical potential of the ions. For $\pi=f_1, f_2, f_3, f_4$, this relation reads:

$$n_i(v_i - v_\pi) = -D_{i\pi} \nabla \mu_i \quad (11)$$

with $D_{i\pi}(\mathbf{x}, t)$ second-order diffusion tensor of the ions diffusing through the interstitial fluid π . It has the unit $\text{m}^2.\text{s}^{-1}$.

The stress-strain relations for the solids, the stress relation for the ions and the stress-velocity relations for the interstitial fluids are elaborated under the classical assumption for heterogeneous media that the Cauchy stress tensor of the total heterogeneous medium is composed of a solid and a fluid part:

$$\sigma = \sigma_{s1} + \sigma_{s2} + \sigma_{s3} + \sigma_{s4} + \sigma_{f1} + \sigma_{f2} + \sigma_{f3} + \sigma_{f4} + \sigma_i \quad (12)$$

with σ the Cauchy stress tensor of the total heterogeneous medium in Pa.

- Stress-strain relations for the solids $\pi=s_1, s_2, s_3, s_4$: under the assumption of small displacements and small strains, the solids are considered as linear isotropic elastic materials and a Hooke's stress-strain relation is taken for each solid

$$\sigma_\pi = D_\pi^e : \varepsilon_\pi \quad (13)$$

with $D_\pi^e(\mathbf{x}, t)$ the elasticity tensor of the solid π in Pa, $\varepsilon_\pi(\mathbf{x}, t)$ the strain tensor of solid π (for $\pi=s_1, s_2, s_3, s_4$) defined by

$$\varepsilon_\pi = \nabla^s u_\pi \quad (14)$$

with $u_\pi(\mathbf{x}, t)$ the displacement field of solid π in m. The superscript s denotes the symmetric part of the gradient operator. For later use in paragraph 5, equation (13) can be rewritten more conveniently with matrix-vector notations:

$$\varepsilon_\pi = E_\pi : \sigma_\pi \quad (15)$$

with

$$E_\pi = (D_\pi^e)^{-1} \quad (16)$$

where $E_\pi(\mathbf{x}, t)$ is the matrix of the elasticity compliances defined as the inverse of the matrix $D_\pi^e(\mathbf{x}, t)$ of the elasticity coefficients. Each component $E_{\pi ij}(\mathbf{x}, t)$ for $i, j \in \{x, y, z\}$ of the elasticity compliance matrix $E_\pi(\mathbf{x}, t)$ is with unit Pa^{-1} . In vector notations, for constituent π (for $\pi=s_1, s_2, s_3, s_4$), the Cauchy stress and the strain are given by:

$$\sigma_\pi(\mathbf{x}, t) = \begin{bmatrix} \sigma_{\pi xx}(\mathbf{x}, t) \\ \sigma_{\pi yy}(\mathbf{x}, t) \\ \sigma_{\pi zz}(\mathbf{x}, t) \\ \sigma_{\pi xy}(\mathbf{x}, t) \\ \sigma_{\pi yz}(\mathbf{x}, t) \\ \sigma_{\pi zx}(\mathbf{x}, t) \end{bmatrix} \quad (17)$$

and

$$\varepsilon_\pi(\mathbf{x}, t) = \begin{bmatrix} \varepsilon_{\pi xx}(\mathbf{x}, t) \\ \varepsilon_{\pi yy}(\mathbf{x}, t) \\ \varepsilon_{\pi zz}(\mathbf{x}, t) \\ \varepsilon_{\pi xy}(\mathbf{x}, t) \\ \varepsilon_{\pi yz}(\mathbf{x}, t) \\ \varepsilon_{\pi zx}(\mathbf{x}, t) \end{bmatrix} \quad (18)$$

with the elasticity compliance matrix in matrix-vector notation:

$$E_\pi(\mathbf{x}, t) = \begin{bmatrix} \frac{1}{E_\pi} & \frac{-\nu_\pi}{E_\pi} & \frac{-\nu_\pi}{E_\pi} & & & \\ \frac{-\nu_\pi}{E_\pi} & \frac{1}{E_\pi} & \frac{-\nu_\pi}{E_\pi} & & & \\ \frac{-\nu_\pi}{E_\pi} & \frac{-\nu_\pi}{E_\pi} & \frac{1}{E_\pi} & & & \\ & & & \frac{1+\nu_\pi}{E_\pi} & 0 & 0 \\ & 0 & & 0 & \frac{1+\nu_\pi}{E_\pi} & 0 \\ & & & 0 & 0 & \frac{1+\nu_\pi}{E_\pi} \end{bmatrix} \quad (19)$$

where $E_\pi(\mathbf{x}, t)$ is the Young modulus of the solid π and $\nu_\pi(\mathbf{x}, t)$ is the Poisson's ratio of the solid π .

- The stress relation for the ions assumes the Cauchy stress tensor of the ions to model a static isotropic stress state defined as

$$\sigma_i = -p_i I \quad (20)$$

with $p_i(\mathbf{x}, t)$ the pressure of the ions in Pa. $p_i(\mathbf{x}, t)$ is equal to the opposite of the osmotic pressure determined by the ions summed to the pressure accounting for solids-ions interactions.

- Stress-velocity relations for the fluids $\pi=f_1, f_2, f_3, f_4$: from now on π refers to the fluids and equals f_1, f_2, f_3, f_4 except if it is stated differently. In our analysis, σ_π is the Cauchy stress tensor of the interstitial fluid π . It represents the surface forces applied on a fluid particle. For interstitial fluids in skin, the Cauchy stress tensor of the interstitial fluid π is a symmetric tensor which can be usually decomposed as

$$\sigma_\pi = \sigma_\pi^{rev} + \sigma_\pi^{irr} \quad (21)$$

where σ_π^{rev} is the reversible part of the Cauchy stress tensor of the interstitial fluid π and σ_π^{irr} is the irreversible part of the Cauchy stress tensor of the interstitial fluid π .

As for the ions, it is assumed that the reversible part of the Cauchy stress tensor σ_π^{rev} is a static isotropic stress state that would exist if the fluid π is at rest and which is usually defined as

$$\sigma_\pi^{rev} = -p_\pi I \quad (22)$$

where the scalar p_π is the interstitial fluid pressure of the interstitial fluid π . Interstitial fluids in skin soft tissues are supposed to be in thermodynamic equilibrium with the thermodynamic fluid pressure function of the relative mass density and the temperature of the interstitial fluid π . In the more general case, it is then necessary to solve an equation for conservation of thermal energy along with momentum and mass conservations. With the assumption of constant temperature, this is not needed here. As a direct consequence it is then possible to identify the interstitial fluid pressure p_π of the interstitial fluid π with the thermodynamic pressure of fluid π i.e. the hydrostatic pressure of liquid in small pores within a matrix of cells, proteins and micro vessels that make up the tissue. This hydrostatic pressure is maintained in a dynamic environment by fluid transfers between the vessels and tissues governed by Starling forces, the contractile forces of cells within the tissue, the microanatomy of the tissue, and the complex mechanical properties of the tissue as a whole [15].

The irreversible part of the Cauchy stress tensor σ_π^{irr} is a viscous stress tensor, corresponding to the part of the stress due to the fluid motion. Additionally, let us consider the interstitial fluids to be Newtonian fluids with shear stresses linearly proportional to the velocity gradient in the direction perpendicular to the plane of shear. In this case, for a compressible Newtonian viscous fluid π the relation between the viscous stress tensor and the velocity gradient given by [33] reads

$$\sigma_\pi^{irr} = 2\widetilde{\mu}_\pi \nabla v_\pi + \widetilde{\eta}_\pi (\nabla \cdot v_\pi) I \quad (23)$$

with $\widetilde{\mu}_\pi(\mathbf{x}, t)$ dynamic viscosity of the interstitial fluid π in Pa.s, $\widetilde{\eta}_\pi(\mathbf{x}, t)$ viscosity coefficient of the interstitial fluid π in Pa.s defined as [34]

$$\widetilde{\eta}_\pi = -\frac{2}{3}\widetilde{\mu}_\pi \quad (24)$$

In our model, we need a relation to calculate the interstitial fluid pressure p_π of each interstitial fluid π . Let us consider that each layer is subjected to an external hydrostatic load $\bar{p}_{mechanical L\pi}$ (for $L\pi=L_1, L_2, L_3, L_4$) applied by the interstitial fluid around combined with the surrounding cells and soft tissue elements. From now on, for simplification of the notations $L\pi=L_1, L_2, L_3, L_4$ except if it is stated differently. For each layer $L\pi$, this mechanical pressure can be expressed as [35]

$$\bar{p}_{mechanical L\pi} = -\frac{1}{3} tr \sigma_{L\pi} \quad (25)$$

or equivalently

$$\bar{p}_{mechanical L\pi} = -\frac{1}{3} tr (\sigma_{s\pi} + \sigma_{f\pi} + \sigma_{i\pi}) \quad (26)$$

with $\sigma_{s\pi}$ Cauchy stress tensor of the solid of layer $L\pi$, $\sigma_{f\pi}$ Cauchy stress tensor of the interstitial fluid of layer $L\pi$ and $\sigma_{i\pi}$ Cauchy stress tensor of the ions present in layer $L\pi$. Reworking relation (26), taking into account relations (20), (21) and (22), leads to

$$p_{f\pi} = \bar{p}_{mechanical\ L\pi} + \frac{1}{3} \text{tr}(\sigma_{s\pi}) + \frac{1}{3} \text{tr}(\sigma_{f\pi}^{irr}) - p_{i\pi} \quad (27)$$

This relation (27) illustrates the differences existing between mechanical and thermodynamic pressures for a layer $L\pi$. In presence of solids and ions, the thermodynamic pressure inside a fluid is not equal to the force applied by the fluid on the exterior surface. The differences come from the solids and the ions stresses and also whether the fluid is supposed ideal or viscous. In reference [15], a similar result is found for a solid saturated by a fluid in case of compression of the fluid. This hydrostatic load may result in a variation of volume of the layer due to possible combined changes in volume of its cells and/or its interstitial fluid. For the cell's wall of layer $L\pi$, it is then possible to define the change in volume per unit volume $e_{L\pi}$, called the volumetric strain as

$$e_{L\pi} = \frac{\delta V}{dV} \quad (28)$$

where δV is the change in volume of the cells of layer $L\pi$ and dV is the initial volume of the cells of layer $L\pi$. Further, for isotropic linear elastic solids, as the cell's wall of layer $L\pi$ are seen here, this volumetric strain $e_{L\pi}$, is defined by the trace of the strain tensor $\epsilon_{s\pi}$ of the solid of layer $L\pi$ and can be written as

$$e_{L\pi} = \text{tr} \epsilon_{s\pi} \quad (29)$$

Let us note that for deriving relation (29), the products of the strains have been neglected since the strains are supposed very small here. Making use of the generalized Hooke's law defined by eq. (15), we can write the volumetric strain $e_{L\pi}$ in terms of the stress state $\sigma_{s\pi}$ of the solid present in layer $L\pi$ and get

$$e_{L\pi} = \text{tr}(E_{s\pi} : \sigma_{s\pi}) \quad (30)$$

where $E_{s\pi}$ is the matrix of the elasticity compliances of the solid present in layer $L\pi$. Rearranging terms in equations (27) and (30) yields for layer $L\pi$

$$\frac{\bar{p}_{mechanical\ L\pi}}{e_{L\pi}} = \frac{p_{f\pi}}{\text{tr}(E_{s\pi} : \sigma_{s\pi})} - \frac{1}{3} \frac{\text{tr}(\sigma_{s\pi})}{\text{tr}(E_{s\pi} : \sigma_{s\pi})} - \frac{1}{3} \frac{\text{tr}(\sigma_{f\pi}^{irr})}{\text{tr}(E_{s\pi} : \sigma_{s\pi})} + \frac{p_{i\pi}}{\text{tr}(E_{s\pi} : \sigma_{s\pi})} \quad (31)$$

The terms on the right consist only of the material properties. It is equal to the ratio of the normal stress $\bar{p}_{mechanical\ L\pi}$ to the volumetric strain $e_{L\pi}$. We recognize in relation (31) the definition of the bulk modulus of elasticity $\tilde{k}_{s\pi}$ of the solid present in layer $L\pi$

$$\frac{\bar{p}_{mechanical\ L\pi}}{e_{L\pi}} = -\tilde{k}_{s\pi} \quad (32)$$

It gives an indication on the stiffness of the volume of material. This bulk modulus needs to be experimentally determined and can be highly variable and quite difficult to obtain. Relation (32) can be reworked taking into account relation (14) and written for layer $L\pi$

$$\bar{p}_{mechanical\ L\pi} = -\tilde{k}_{s\pi} \text{tr}(\nabla^s u_{s\pi}) \quad (33)$$

with $u_{s\pi}$ displacement field of the solid present in layer $L\pi$. Using relations (13), (14), (23), (24), (27), (29) and (33), it comes for layer $L\pi$:

$$p_{f\pi} = -\tilde{k}_{s\pi} \text{tr}(\nabla^s u_{s\pi}) + \frac{1}{3} \text{tr}(D_{s\pi}^e : \nabla^s u_{s\pi}) + \frac{2}{3} \tilde{\mu}_{f\pi} \{ \text{tr}(\nabla v_{f\pi}) - (\nabla \cdot v_{f\pi}) \} - p_{i\pi} \quad (34)$$

where $\tilde{\mu}_{f\pi}$ and $v_{f\pi}$ are respectively the dynamic viscosity and the velocity field of the interstitial fluid present in layer $L\pi$. Hence this relation (34) makes it possible to calculate the interstitial fluid pressure within a linear isotropic elastic material, provided knowledge on the displacement field of the solid, on the bulk mechanical properties of the solid, on the velocity field of the interstitial fluid and on the mechanical properties of the interstitial fluid.

The field equations, i.e. the balance of mass for the solids, the fluids and for the ions, the balance of momentum for the solids, the fluids and the ions, the material relations for the solids, the fluids and the ions, are complemented by the boundary conditions which hold on complementary parts of the boundary in terms of prescribed external traction or prescribed displacement for the solids, prescribed outflow of fluids or prescribed chemical potential for the fluids and prescribed outflow of ions or prescribed chemical potential for the ions respectively. The initial conditions which specify the displacements u_π for the solids $\pi=s_1, s_2, s_3, s_4$, the velocities v_π for the solids $\pi=s_1, s_2, s_3, s_4$ and the chemical potentials μ_π for the fluids and the ionic component $\pi=f_1, f_2, f_3, f_4, i$ at time $t=0$ close the initial value problem.

4 Experimental device

The original LTDS-indentation device (Fig. 3) developed by the team of Prof. H. Zahouani is used here to evaluate the mechanical properties of the different skin layers. The main advantage of this indenter is to be fixed to a rigid arm able to move with respect to a fixed rigid heavy support. Therefore it is not necessary to tie the indenter to the human body during the experiments and to disturb the natural stress state of the skin before application of the mechanical load. The experimental set-up is presented in Figure 4 [26].



FIGURE 3: Original LTDS-indentation device.

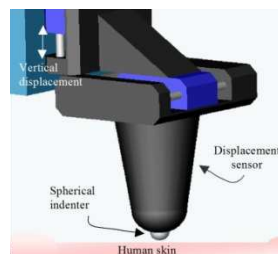


FIGURE 4: Experimental set-up of the LTDS-indentation device.

During an experiment, the indenter is manually positioned near the skin outer surface. Then a controlled normal force F_{load} is applied onto the outer surface of the skin by means of the rigid spherical indenter (diameter 6 mm) of the indentation device.

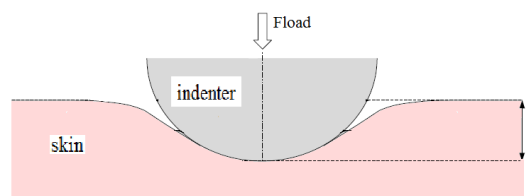


FIGURE 5: Typical contact profile developed during indentation: h is the indentation depth, F_{load} is the applied load [30]

The use of a spherical indenter insures that there is no deterioration of the skin surface and therefore no penetration of the indenter. The total response of the skin will be the composite response of the individual contributions of the stratum corneum, the viable epidermis, the dermis and the hypodermis.

A contact profile of the overall answer of the different skin layers develops of the form given in Fig 5 with possible sink-in or pile-up of the skin at the vicinity of the indenter given in Fig 6.

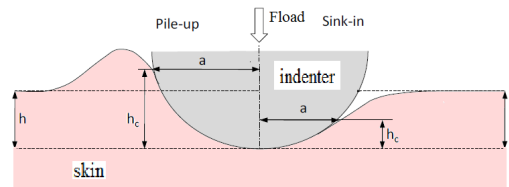


FIGURE 6: Typical contact profile developed during indentation when the surface of the skin sinks in or piles-up: h indentation depth, F_{load} applied load, a contact radius, h_c contact depth [30]

The indentation depth h of the spherical indenter is recorded as a function of this normal applied force, F_{load} , during loading-unloading experiments. The recorded curve for an indentation test performed on the volar forearm zone of a volunteered young healthy adult is given in figure 7. The chosen location makes the indentation tests less tiring for the volunteer because of the position of the arm resting on a support during the test and therefore the recorded data are less disturbed by the natural movement of the body. The indentation test is realized for a constant indentation speed of $500.0 \mu\text{m/s}$ at ambient temperature and without surface treatment on skin before the test. Figure 7 displays a quite reversible loading-unloading experimental curve with a very low hysteresis. In addition, no residual print was seen onto the surface of the skin after the experiment. These observations are coherent with the choice made for this analysis to model human skin soft tissues as elastic materials in this load range.

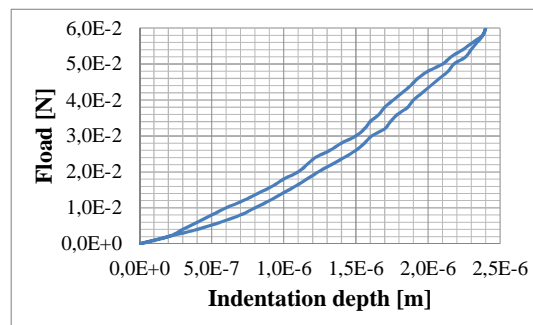


FIGURE 7: Recorded curve for a loading-unloading indentation test performed on the volar forearm of a young adult.

The numerical simulations, presented here after in paragraph 5, aim to reproduce this experimentation in order to help characterizing *in vivo* equivalent mechanical parameters of human skin soft tissues. The recorded curve will provide the loading-unloading steps of the numerical simulations as well as physically admissible boundary and initial conditions. For that purpose, the recorded experimental curve (Fig. 7) is reworked to obtain a curve of the applied mechanical load F_{load} versus time (Fig. 8). During the loading steps, the load is applied gradually from 0 N to $6.0\text{E-}2 \text{ N}$ from 0 s to $4.8\text{E-}3 \text{ s}$. Then for the unloading steps, the load is decreased slowly from $6.0\text{E-}2 \text{ N}$ to 0 N from $4.8\text{E-}3 \text{ s}$ to $9.6\text{E-}3 \text{ s}$.

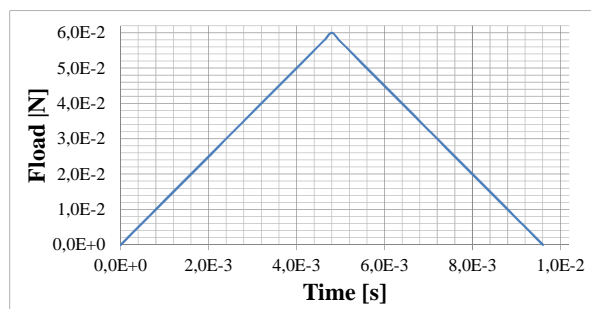


FIGURE 8: Applied mechanical load F_{load} versus time for the loading-unloading steps of the numerical simulations

5 Numerical simulation

5.1 Finite difference model

The nine non-linear systems of equations written in section 3 for all the nine constituents of the skin specimen are dealt with by a 1-dim finite difference analysis. It provides insights in the couplings and influences of fluid flows triggered by ions transport under applied mechanical loads. The spatial derivatives appearing in the field equations and the material relations are approximated with a second-order accurate finite difference scheme. Explicit forward finite differences are used to approximate the temporal derivatives, which are first-order accurate. The fundamental unknowns are the displacement of the solids, the volumic ratios of the fluids and the concentration of the ions. The incremental material relations for the solids, the fluids and the ions give directly the increment of their associated variable.

All calculations are carried out for a specimen of skin for which an estimate of the thickness of the skin inner forearm zone is needed. This has not been measured during the experimentation. Therefore it is assumed in the numerical simulation that the thickness of the skin at this part (stratum corneum + viable epidermis + dermis + hypodermis) is approximately 1516 μm (12 μm for the stratum corneum + 102 μm for the viable epidermis + 1002 μm for the dermis + 400 μm for the hypodermis). This estimation is coherent with respect to [36, 29]. This skin specimen is meshed with 380 elements (Fig. 9). The space increment equals 4 μm and is assumed to be uniform within each layer and for all the skin specimen. The time increment needed to model the loading-unloading steps is taken equal to 1.6E-4 s. As remarked in a previous work, the choice of these increments is motivated by convergence needs [37]. A set of material parameters, taken as mean values for human skin available in the literature [32], complements the model except as regards of the mechanical parameters for which a mechanical parameters estimation procedure is carried out in paragraph 5.2.

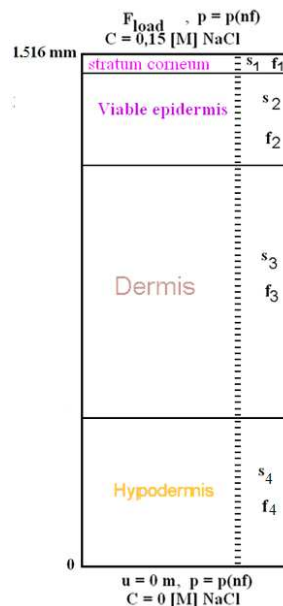


FIGURE 9: Finite difference mesh and boundary conditions

5.2 Mechanical parameters estimation procedure

The mechanical parameters, here the elastic moduli E_{S1} , E_{S2} , E_{S3} and E_{S4} for respectively the stratum corneum, the viable epidermis, the dermis and the hypodermis, are estimated by fitting the loading

branch of the experimental load-displacement curve (Fig. 7) following an iterative procedure. The input file provides the finite difference program with a set of parameters including trial mechanical parameters as well as the applied load (Fig. 8). Then the calculus runs. The computed skin surface displacements during the loading steps are extracted from the calculated numerical results and compared with the experimentally obtained axial displacement of the skin surface under the indenter. Figure 10 displays the comparison between the experimental displacement curve and the numerically obtained surface displacements curves for various combinations of discrete values of the mechanical parameters for all layers. The curve “SC1925000 VE1200 DE4000 HY2000” corresponds to a simulation carried out with elastic moduli of $E_{S1}=1925.0E3$ Pa for the stratum corneum, $E_{S2}=1.2E3$ Pa for the viable epidermis, $E_{S3}=4.0E3$ Pa for the dermis and $E_{S4}=2.0E3$ Pa for the hypodermis and where SC, VE, DE and HY refers respectively to the stratum corneum, the viable epidermis, the dermis and the hypodermis. The curve “SC2475000 VE1200 DE4000 HY2000” corresponds to a simulation carried out with elastic moduli of $E_{S1}=2475.0E3$ Pa for the stratum corneum, $E_{S2}=1.2E3$ Pa for the viable epidermis, $E_{S3}=4.0E3$ Pa for the dermis and $E_{S4}=2.0E3$ Pa for the hypodermis. The curve “SC2925000 VE1200 DE4000 HY2000” corresponds to a simulation carried out with elastic moduli of $E_{S1}=2925.0E3$ Pa for the stratum corneum, $E_{S2}=1.2E3$ Pa for the viable epidermis, $E_{S3}=4.0E3$ Pa for the dermis and $E_{S4}=2.0E3$ Pa for the hypodermis. A least squares approach gives the minimum difference between experimental and numerical results. The comparison shows a best fit at approximately the curve “SC2475000 VE1200 DE4000 HY2000”.

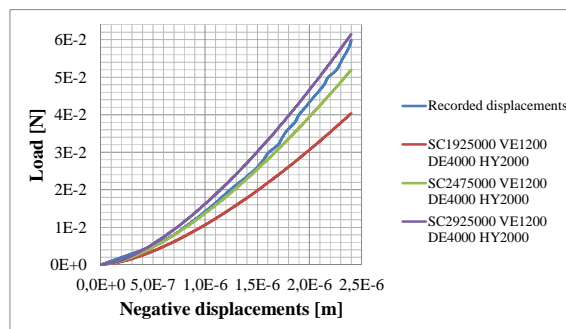


FIGURE 10: Comparison between numerical displacements curves and the experimental displacement curve for various combinations of mechanical parameters.

5.3 Numerical model

The four layers of skin soft tissues are modelled as isotropic linear elastic materials saturated by a Newtonian viscous fluid with the following material parameters [32]:

- as found in sub-section 5.2, an elastic modulus of $E_{S1}=2475.0E3$ Pa for the stratum corneum-simulating solid s1, $E_{S2}=1.2E3$ Pa for the viable epidermis-simulating solid s2, $E_{S3}=4.0E3$ Pa for the dermis-simulating solid s3 and $E_{S4}=2.0E3$ Pa for the hypodermis-simulating solid s4.
- the dynamic viscosities are taken equal to $\widetilde{\mu}_{f1} = 1.002E-3$ Pa.s for the stratum corneum-simulating interstitial fluid f1, $\widetilde{\mu}_{f2} = 2.0E-3$ Pa.s for the viable epidermis-simulating interstitial fluid f2, $\widetilde{\mu}_{f3} = 3.0E-3$ Pa.s for the dermis-simulating interstitial fluid f3 and $\widetilde{\mu}_{f4} = 3.5E-3$ Pa.s for the hypodermis-simulating interstitial fluid f4;
- an absolute mass density $\rho'_{\pi} = 1330.0$ kg.m⁻³ is assumed for each solid $\pi = s_1, s_2, s_3, s_4$;
- an absolute mass density $\rho'_f = 1000.0$ kg.m⁻³ is adopted for each of the four interstitial fluids;
- for the ions, an absolute mass density $\rho'_i = 1549.0$ kg.m⁻³ is taken.
- in the calculations, the permeability $K = 1.98E-21$ m⁴.N⁻¹.s⁻¹ and the diffusion coefficient $D_i = 3.3E-11$ m².s⁻¹ are adopted.

The boundary conditions deduced from the experimentation are given in Figure 9 and translated here after in terms of the physical variables of the theoretical model:

- For the external upper skin surface: a force is applied at the outer upper skin surface node equivalent to the imposed indentation load obtained from the experimental curve (Figure 8), fluid pressures equal to the atmospheric pressure are imposed, the skin surface is in contact with a 0.15 [M] NaCl solution [32] with no continuous supply.

- For the inward skin surface: the inward lower surface node is subjected to a displacement condition of 0 mm displacement, fluxes of fluids are set to zero, a zero flux of ions is imposed. These boundary conditions on the fluids and the ions express that these constituents are prevented from flowing outside the skin specimen. This means that here interstitial fluids are supposed not to flow freely through the inward skin surface downward through the underlying muscle.

In the initial state, all layers are considered made out of fully saturated material with no ionic component i.e. the volumic ratio of the ions is set equal to zero for all the layers in the initial state. The calculus starts with an initial state based on experimental data or fit given in [32].

6 Results and discussion

At the end of the computation, the numerical simulations give the evolutions of all the state variables for all the constituents with respect to space and time. They are given and discussed here after for some variables in terms of profiles along the specimen of skin in vivo for five steps of calculations $t = 3.2E-4$ s, $2.4E-3$ s, $4.8E-3$ s, $7.2E-3$ s and $9.6E-3$ s.

The volumic ratios of the ions are given in Figure 11 for 3 steps of calculations $t = 3.2E-4$ s, $2.4E-3$ s and $4.8E-3$ s for the upper sub-layers of skin soft tissues where the ions have penetrated. The other layers are still without ions. The ions deposited at the outer upper surface of the stratum corneum are penetrating through the stratum corneum and also through the first sub-layers of the viable epidermis till sub-layer with node with coordinate $13.92E-4$ m. While the ions are penetrating, the volumic ratios are increasing with time with for example a volumic ratio equating $3.89E-8$ at time $2.4E-3$ s and $1.24E-7$ at time $4.8E-3$ s for the sub-layer-simulating node with coordinate $15.04E-4$ m.

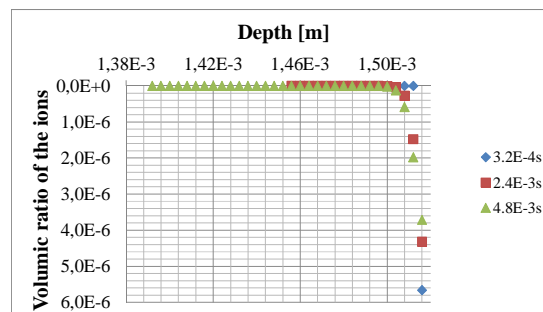


FIGURE 11: Volumic ratio of the ions
(zoom on the upper sub-layers where the ions have penetrated)

The velocity of the ions are given in Figure 12 for the same 3 steps of calculations $t = 3.2E-4$ s, $2.4E-3$ s and $4.8E-3$ s for the upper layers of skin soft tissues. The other layers are remaining without ions. It appears that while the ions are penetrating, the order of magnitude of the absolute value of their velocity is decreasing quite a lot. For instance, the velocity passes from $-5.74E-4$ m.s⁻¹ at time $2.4E-3$ s to $-2.55E-4$ m.s⁻¹ at time $4.8E-3$ s for the sub-layer-simulating node with coordinate $15.04E-4$ m.

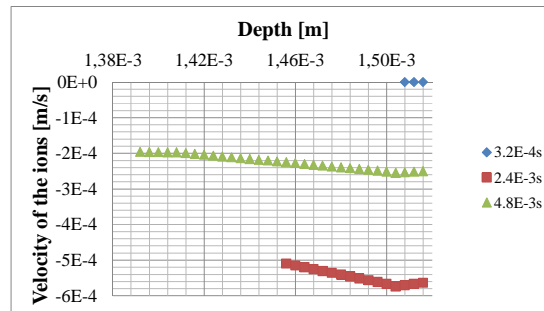


FIGURE 12: Velocity of the ions
(zoom on the upper sub-layers where the ions have penetrated)

Figure 13 displays the linear profiles of the volumic ratios of the fluids for the five steps of calculations. The curves are overlapping because of very small evolutions with respect to time. For example for the sub-layer-simulating node with coordinate $15.04E-4$ m, the volumic ratio equals $131.167E-3$ at time $2.4E-3$ s and $131.194E-3$ at time $9.6E-3$ s.

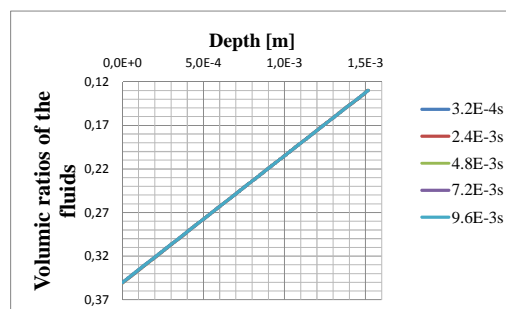


FIGURE 13: Volumic ratios of the fluids

The associated profiles of the velocities of the fluids are given in Figure 14. They exhibit very different kinetics with respect to time and depending on the layer. This has a significant influence on the displacements of the solids. During the mechanical loading steps (from 0 s to $4.8E-3$ s), the velocities are negative for all nodes of the mesh. The fluids are flowing inward from the upper outer surface of the stratum corneum till the bottom sub-layers of the hypodermis. For example velocities equal $-2.55E-4$ m.s⁻¹ for the sub-layer-simulating node with coordinate $15.16E-4$ m and $-1.08E-6$ m.s⁻¹ for the sub-layer-simulating node with coordinate $4.00E-6$ m at time $4.8E-3$ s. Then the velocities are becoming positive for all nodes of the mesh during the mechanical unloading steps ($4.8E-3$ s to $9.6E-3$ s). This change shows fluids flowing back in the opposite direction. For example velocities equal $10.20E-4$ m.s⁻¹ for the sub-layer-simulating node with coordinate $15.16E-4$ m and $3.51E-6$ m.s⁻¹ for the sub-layer-simulating node with coordinate $4.00E-6$ m at time $9.6E-3$ s.

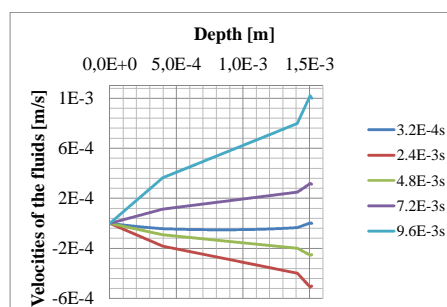


FIGURE 14: Velocities of the fluids

Figure 15 shows the interstitial fluids pressures versus the volumic ratios of the fluids at the beginning of the loading steps i.e. before any external mechanical load is applied at the top outer surface of the skin specimen. It is worth to remark the order of magnitude of these pressures varying between $[-6.6E+7 ; -1.6E+7]$ Pa depending on the sub-layer-simulating node. This means that the presented model is able to translate the initial conditions deduced from the experimentation procedure and to

give non-zero interstitial fluids pressures all along the skin specimen with order of magnitude in the range found in [32].

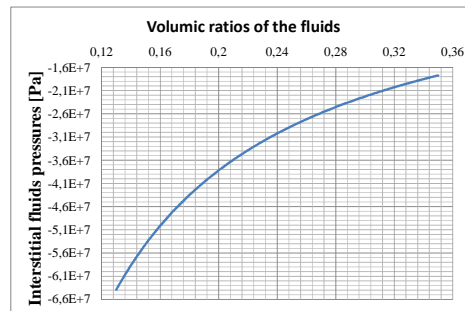


FIGURE 15: Interstitial fluids pressures versus the volumic ratios of the fluids at the beginning of the loading steps

Moreover, Figure 16 displays the profiles of the interstitial fluids pressures along the skin specimen for the five steps of calculations. The pressures are not remaining constant during the loading-unloading steps. They exhibit very small variations with respect to time. For example pressures equal $-6136.9544E+4$ Pa at time $3.2E-4$ s, $-6124.7379E+4$ Pa at time $2.4E-3$ s, $-6116.5502E+4$ Pa at time $4.8E-3$ s, $-6121.4119E+4$ Pa at time $7.2E-3$ s and $-6132.3828E+4$ Pa at time $9.6E-3$ s for the sub-layer-simulating node with coordinate $14.84E-4$ m. In spite of the couplings with the other variables appearing in the model, the pressures are facing the fluctuations of these variables and remain in tied limits. The order of magnitude of these interstitial fluids pressures are similar to the ones given in [32].

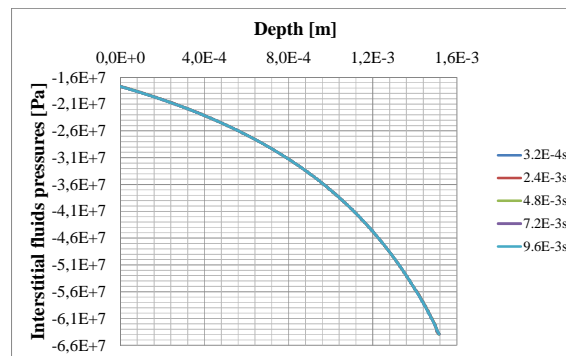


FIGURE 16: Interstitial fluids pressures

The negative displacements of the solids are presented in Figure 17. During the mechanical loading steps (0 s to $4.8E-3$ s), the solids tend to consolidate all along the specimen of skin soft tissues. On the contrary during the mechanical unloading ($4.8E-3$ s to $9.6E-3$ s), the different layers expand in all the specimen of skin. Both for the loading and the unloading steps, different orders of magnitude are found depending on the layer. For example the displacements equal $-20.349E-8$ m at time $3.2E-4$ s, $-15.910E-7$ m at time $2.4E-3$ s, $-24.481E-7$ m at time $4.8E-3$ s, $-17.340E-7$ m at time $7.2E-3$ s and $-20.354E-8$ m at time $9.6E-3$ s for the sub-layer-simulating node with coordinate $15.04E-4$ m. It should be noted that thanks to the relation (34) derived for describing the interstitial fluid pressure of each interstitial fluid, in this analysis with the choice of isotropic linear elastic behavior for the different skin tissues-simulating solids, the state at the end of the unloading steps has come back to the initial one (curve at time $3.2E-4$ s and curve at time $9.6E-3$ s are overlapping each other).

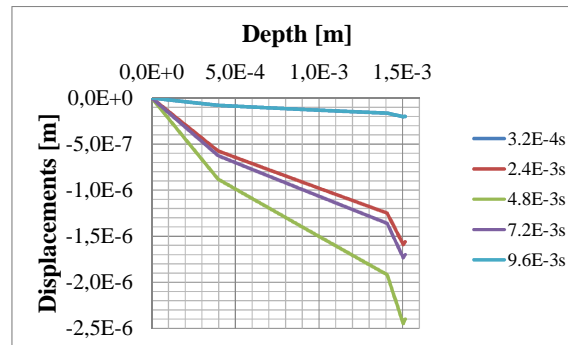


FIGURE 17: Displacements of the solids

In vivo, in its initial state before experiment, human skin is the place of physiological influences such as transports of small solutes through membranes, water flows from high concentrations to low ones, variations of permeability, ... This makes that physiological fluids are constantly flowing, equilibrium is never reached. Because of this net movement of physiological fluids, the studied specimen of human skin is not in equilibrium at the beginning of the loading steps with respect to the fluids. This has an important consequence on the interstitial fluids pressures which are not equal to zero at the beginning of the calculations. Thanks to relation (34), the present model is able to compute these non-zero interstitial fluids pressures as shown in Figure 15.

Moreover, Figure 18 gives the comparison between the experimental displacement curve, the computed surface displacements curve obtained with the model without relation (34) as given in reference [27] and the computed surface displacements curve obtained with the present model with relation (34). The model with relation (34) is able to handle non-zero interstitial fluids pressures and to retrieve that a zero applied mechanical load F_{load} leads to a zero computed numerical penetration depth as found experimentally.

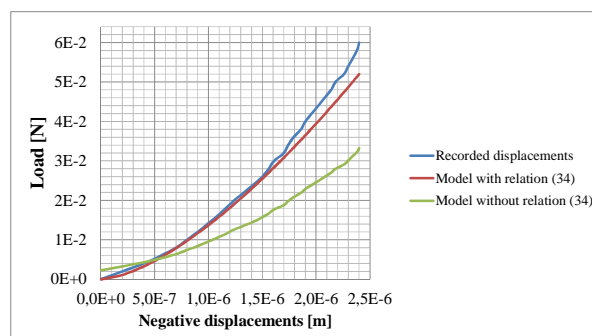


FIGURE 18: Comparison between numerical displacements curves and the experimental displacement curve for the skin model with and without relation (34).

The determined estimates of the mechanical parameters of each layer, i.e. $E_{S1}=2475.0E3$ Pa for the stratum corneum, $E_{S2}=1.2E3$ Pa for the viable epidermis, $E_{S3}=4.0E3$ Pa for the dermis and $E_{S4}=2.0E3$ Pa for the hypodermis lead to qualitatively physically admissible evolutions for the specimen of human skin subjected to mechanical loadings, when compared with other observations of indentation tests [26, 29]. Moreover it is worth to notice that these values remain in the intervals that can be found in the literature [18, 19, 20].

With its strong tensile strength coming from the brick-and-mortar structure of hard keratinized dead cells and lipid, the stratum corneum reacts transmitting the received external mechanical load. At the same time, ions start penetrating through the stratum corneum. Parts of the mechanical load are transmitted to the souple viable epidermis. The soft living cells of this layer experiment a consolidation-type behavior, taking a big part of the transmitted mechanical load. This behavior of the viable epidermis influences the driving forces governing the transport of the ions which will penetrate till the viable epidermis. Although the ions are not going further inward in spite of the skin surface still in contact with the remaining of the NaCl solution. The ions will tend to accumulate and to exchange

with the surroundings in this sub-layer. A part of transmitted mechanical external load is now arriving to the dermis. There, the gel combines with the collagen and elastin fibers to protect the soft living cells from being damaged. First the gel acts as a protective cocoon till a yield pressure. Then the interwoven collagen fibers and the rubber-like elastin fibers will provide strength and elastic behavior. These coupled behaviors of the solid of the dermis and the gel lead to a consolidation-type behavior of the dermis with a magnitude lower than the one of the viable epidermis. The last part of transmitted mechanical external load ends to be handled by the loose fatty cells of the hypodermis. This layer reacts almost like a rubber mattress with a reversible behavior. With respect to the physiological fluids bathing the different layers of skin soft tissues, the obtained numerical results show physiological fluid pressures influenced by the couplings between ions-fluids-solids behaviors as well as by the external mechanical applied load and the presence of the NaCl solution because they face small evolutions. However these physiological fluid pressures are also kept between physically admissible limits. They do not exceed living pressures that can be recorded during in vivo experimentations [32].

7 Conclusion

This paper has presented a tri-phasic skin model where skin is composed of four solids, four interstitial fluids and an ionic component. In this model, the skin soft tissues are treated as elastic linear isotropic materials while the interstitial fluids are considered as Newtonian viscous fluids. A relation is proposed for estimating interstitial fluid pressures. This model makes it possible to follow the interstitial flow of fluids coupled with the transport of ions influenced by external mechanical loads and also to study their influence on the deformations of the solids describing skin soft tissues. The numerical simulation of indentation experiment gives an estimate of the Young modulus of each layer, i.e. $E_{S1}=2475.0E3$ Pa for the stratum corneum, $E_{S2}=1.2E3$ Pa for the viable epidermis, $E_{S3}=4.0E3$ Pa for the dermis and $E_{S4}=2.0E3$ Pa for the hypodermis. These estimates are thought to be physically reasonable when compared to values available in the literature because they lead to qualitatively good agreement between experimental observations and the numerical descriptions of the overall response of the skin specimen obtained here.

Références

- [1] G. Odland, Structure of the skin, Physiology, biochemistry and molecular biology of the skin, L.A. Goldsmith (ed.), Oxford University Press, Oxford, 1991.
- [2] J. Ginefri, I. Darasse, P. Crozat. High-temperature superconducting surface coil for in vivo microimaging of the human skin, *Magnetic Resonance in Medicine*, 45, pp. 376-382, 2001.
- [3] G. Wilkes, I. Brown, R. Wildnauer. The biomechanical properties of skin, *Critical Reviews in Bioengineering*, pp. 453-495, 1973.
- [4] E. H. Starling. On the absorption of fluids from the connective tissue spaces. *J. Physiol. Sci.*, 19, pp. 312-326, 1896.
- [5] D. Negrini, A. Moriondo. Lymphatic anatomy and biomechanics, *J. Physiol.*, 589, 12, pp. 2927-2934, 2011.
- [6] D.C. Zawieja. Contractile physiology of lymphatics. *Lymphat. Res. Biol.*, 7, pp. 87-96, 2009.
- [7] K. Aukland, G. Nicolaysen. Interstitial fluid volume: local regulatory mechanisms. *Physiol. Rev.* 61, pp. 556-643, 1981.
- [8] X. Hu, R.H. Adamson, B. Liu, F.E. Curry, S. Weinbaum. Starling forces that oppose filtration after tissue oncotic pressure is increased. *Am. J. Physiol. Heart Circ. Physiol.*, 279, H1724-H1736, 2000.
- [9] J.R. Levick, C.C. Michel. Microvascular fluid exchange and the revised Starling principle. *Cardiovasc. Res.*, 87, pp. 198-210, 2010.
- [10] R.K. Reed, K. Rubin. Transcapillary exchange: role and importance of the interstitial fluid pressure and the extracellular matrix. *Cardiovasc. Res.*, 87, pp. 211-217, 2010.

- [11] K. Aukland, R.K. Reed. Interstitial-lymphatic mechanisms in the control of extracellular fluid volume. *Physiol. Rev.* 73, pp. 1–78, 1993.
- [12] H. Wiig, O. Tenstad, P.O. Iversen, R. Kalluri, R. Bjerkvig. Interstitial fluid: the overlooked component of the tumor microenvironment? *Fibrogenesis Tissue Repair*, pp. 3-12, 2010.
- [13] J.M. Rutkowski, C.E. Markhus, C.C. Gyenge, K. Alitalo, H. Wiig, M.A. Swartz. Dermal collagen and lipid deposition correlate with tissue swelling and hydraulic conductivity in murine primary lymphedema. *Am. J. Pathol.*, 176, pp. 1122–1129, 2010.
- [14] H. Yao, W.Y. Gu. Three-dimensional inhomogeneous triphasic finite-element analysis of physical signals and solute transport in human intervertebral disc under axial compression. *J. Biomech.*, 40, pp. 2071–2077, 2007.
- [15] A.L. Darling, P.K. Yalavarthy, M.M. Doyley, H. Dehghani, B.W. Pogue. Interstitial fluid pressure in soft tissue as a result of an externally applied contact pressure. *Phys. Med. Biol.*, 52, pp. 4121–4136, 2007.
- [16] M. Soltani, P. Chen. Numerical Modeling of Fluid Flow in Solid Tumors. *PLoS ONE* 6(6): e20344. doi:10.1371/journal.pone.0020344, 2011.
- [17] J.L. Leveque, J. de Rigal, P.G. Agache, C. Monneur, Influence of ageing on the in vivo extensibility of human skin at a low stress, *Archives of Dermatological Research*, 269 (2), pp. 127-135, 1980.
- [18] J.D. Rigal, J. Lévêque, In vivo measurement of the stratum corneum elasticity, *Bioengineering and the Skin*, 1, pp. 13-23, 1985.
- [19] A. Rochefort, Propriétés biomécaniques du stratum corneum : - Modélisation rhéologique – Application à la cosmetology, Thèse de Doctorat, Université de Franche-Comté – Besançon, 1986.
- [20] P. Agache, C. Monneu, J. Lévêque, J. De Rigal, Mechanical properties and young's modulus of human skin in vivo. *Archives of Dermatological Research*, 269, pp. 221-232, 1980.
- [21] C. Daly, Biomechanical properties of dermis, *The Journal of Investigative Dermatology*, 79, pp. 17-20, 1982.
- [22] J. Manschot, A. Brakkee, The measurement and modelling of the mechanical properties of human skin in vivo – i. the measurement, *Journal of Biomechanics*, 19 (7), pp. 511-515, 1986.
- [23] C. Escoffier, J. de Rigal, A. Rochefort, R. Vasselet, J. Lévêque, P. Agache, Age-related mechanical properties of human skin : An in vivo study, *The Journal of Investigative Dermatology*, 93, pp. 353-357, 1989.
- [24] A. Barel, W. Courage, P. Clarys, Suction method for measurement of skin mechanical properties : the Cutometer, *Handbook of Non-Invasive Methods and the skin*, J. Serup and G B E. Jemec (eds), Boca Raton, CRC Press, 1995.
- [25] C. Pailler-Mattei, H. Zahouani, Analysis of adhesive behaviour of human skin in vivo by indentation, *Tribol. Int.*, pp. 12-21, 2006.
- [26] C. Pailler-Mattei, C. Bec, H. Zahouani, In vivo measurements of the elastic mechanical properties of human skin by indentation tests, *Medical Engineering and Physics*, 30, pp. 599-606, 2008.
- [27] M-A. Abellan, H. Zahouani, J-M. Bergheau. Contribution to the Determination of In Vivo Mechanical Characteristics of Human Skin by Indentation Test. *Computational and Mathematical Methods in Medicine*, Volume 2013, Article ID 814025, 11 pages, 2013.
- [28] H. Wiig, R.K. Reed, O. Tenstad. Interstitial fluid pressure, composition of interstitium, and interstitial exclusion of albumin in hypothyroid rats. *Am. J. Physiol. Heart Circ. Physiol.*, 278, H1627-H1639, 2000.
- [29] F.M. Hendriks. Mechanical behaviour of human epidermal and dermal layers in vivo, Dissertation, Eindhoven University of Technology, 2005.
- [30] M. Geerligs, Skin layer mechanics, Dissertation, Eindhoven University of Technology, 2009.
- [31] P. Jouanna, M-A. Abellan, A generalized approach to heterogeneous media, *Transport in Porous Media*, 25, pp. 351-374, 1996.
- [32] P.M. Van Kemenade, Water and ion transport through intact and damaged skin, Dissertation, Eindhoven University of Technology, 1998.
- [33] G.G. Stokes. On the theories of internal friction of fluids in motion. *Trans. Camb. Phil. Soc.*, 8, pp. 287–305, 1845.
- [34] B.R. Bird, W.E. Stewart, E.N. Lightfoot. *Transport phenomena*. John Wiley & Sons, New-York, Chichester, Brisbane, Toronto, Singapore, 1960.

- [35] P. Germain. *Cours de mécanique des milieux continus. Théorie Générale. Tome 1*, Masson et Cie Editeurs, 1973.
- [36] P. Agache, *Physiologie de la peau et exploitations fonctionnelles cutanées*, Editions médicales Internationales, Paris, 2000.
- [37] M-A. Abellan, H. Zahouani, E. Feulvarch, J-M. Bergheau, Modelling water and ion transport through damaged skin, 2nd Euro-Mediterranean Conference on Bioengineering and Biomaterials (EMCBB), July 4-6, Fez, Morocco, 2012.